Journal of Chromatography, 295 (1984) 1–11
Elsevier Science Publishers B.V., Amsterdam — Printed in The Netherlands

CHROM. 16,763

LAMINAR FLOW EFFECTS IN THE COIL PLANET CENTRIFUGE

FREDERICK T. HERRMANN
Separation Processes Branch, Space Science Laboratory, Marshall Space Flight Center, Huntsville, AL 35812 (U.S.A.)

(First received January 6th, 1984; revised manuscript received March 20th, 1984)

SUMMARY

The coil planet centrifuge designed by Ito employs flow of a single liquid phase, through a rotating coiled tube in a centrifugal force field, to provide a separation of particles based on sedimentation rates. Mathematical solutions are derived for the linear differential equations governing particle behavior in the coil planet centrifuge device. These solutions are then applied as the basis of a model for optimizing particle separations.

INTRODUCTION

The purpose of this paper is to improve separations of cells and small particles with the coil planet centrifuge by predicting elution rates of particles based on particle densities, buffer densities, buffer viscosities, buffer flow-rates and centrifugal fields. The understanding of these variables on particle separations will allow a finer adjustment of these operational parameters, thus facilitating better particle separations.

The coil planet centrifuge[1] offers a relatively gentle method for separating cells under a low centrifugal force in a physiological medium which preserves the viability of the cells. In addition to separating small particles such as erythrocytes on the basis of differences in sedimentation rates, this mechanical system provides a means of partitioning cells and macromolecules with aqueous–aqueous polymer phase systems[2].

The non-synchrous flow through coil planet centrifuge allows continuous elution of cell particles through the coiled column without the use of rotating seals. The rotation and revolution rates are independently adjustable. This adjustability of rotational speeds allows proper sedimentation of less dense cell particles. The present apparatus requires no rotating seals thus eliminating the possibility of leakage, contamination, and corrosion.

Fig. 1a is a cross-sectional view through the central axis of the coil planet centrifuge. The use of motors I and II allows independent adjustment of centrifugal field and coil rotation. The column including the inlet and outlet tubing consists of a continuous PTFE tube, 19 m in length, helically wrapped 600 turns about steel tubing. The rotary frame I shown in Fig. 1a depicts the gearing necessary for inde-

0021-9673/84/$03.00

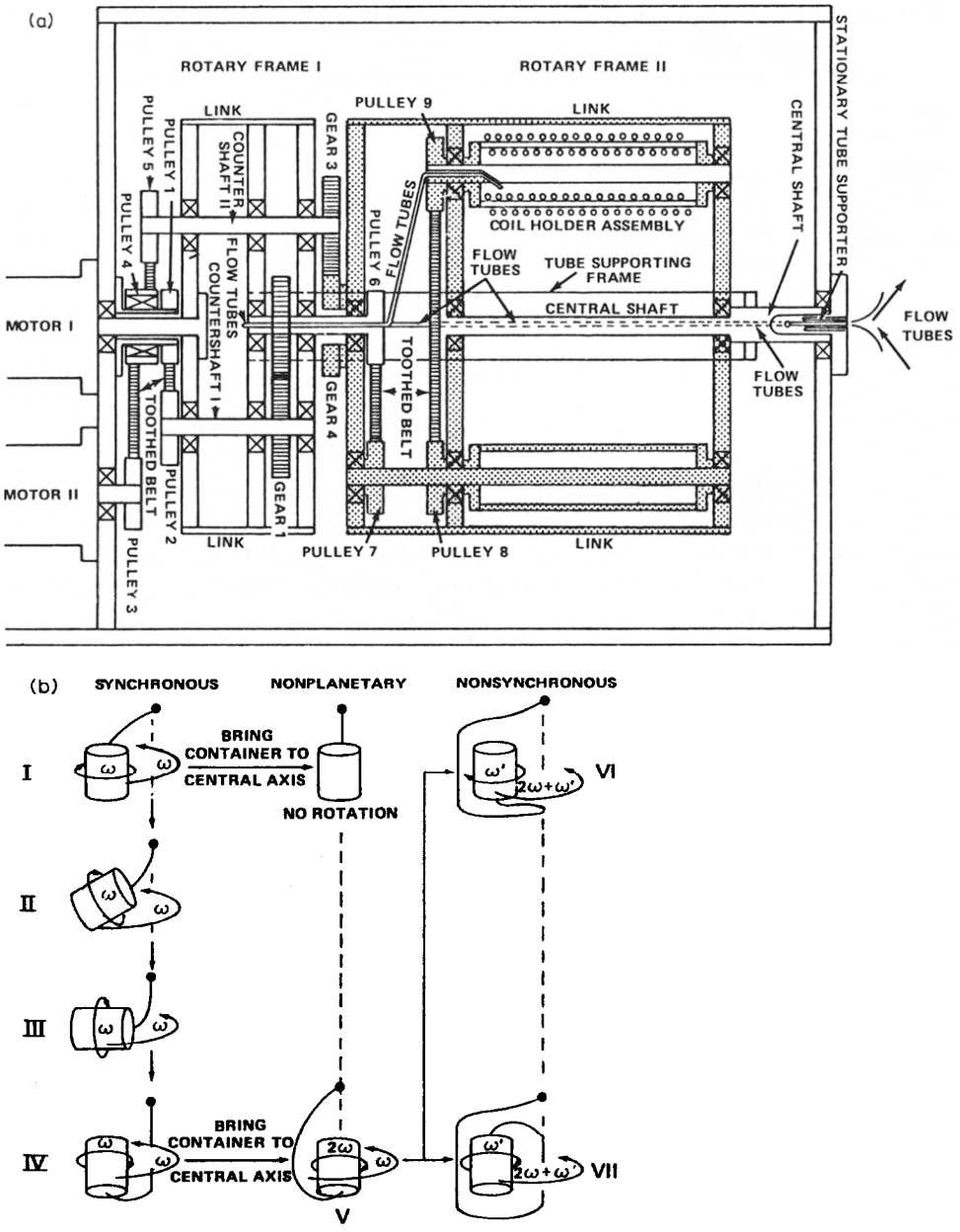

Fig. 1. (a), Cross-sectional view of the nonsynchronous flow-through coil planet centrifuge. (b), Coil planet centrifugation modes. (The figures are used with permission of Y. Ito, Bethesda, MD, U.S.A.)

pendent adjustment of centrifugal field and rotation of the coil holder assembly within the field. In its present configuration, the coiled tubing is filled with isotonic phosphate buffer[1]. After injecting the sample particles to be separated, the coiled tube is rotated slowly around its horizontally oriented axis in the gravitational ac-

celeration field. The flow through buffer mechanism allows continuous fractionation of the samples based on their respective sedimentation rates. The centrifugal force accelerates the sedimentation of cell particles. The particles with higher sedimentation rates are retained longer in the coiled tube as opposed to particles with lesser sedimentation rates which are eluted earlier. Particles with densities greater than the liquid buffer will move toward the end of the coil known as the head[3].

Various types of coil planet centrifugation schemes illustrated in Fig. 1b show the orientation and motion of the column. These separation schemes are divided into three modes of planetary motion. The mode of non-synchronous coil planet centrifugation discussed will be that of scheme VI in which the coil is moved away from the central axis and undergoes a non-synchronous planetary motion.

A theoretical model of small particle dynamics and associated fluid effects upon particle retention times are presented in this paper. Particles with greater sedimentation rates are retained in the coiled tube for a longer period of time. The axial movement of particles within the tube was described by Ito and co-workers[1,4] as being caused by an Archimedean screw force. They neglected, as a first approximation, any lateral motion of particles within the tubing. The model presented in this paper describes particle separation by assuming axial laminar flow velocities determined by the particles lateral position within the coiled tube.

THEORETICAL

For the purpose of this study, two right-handed coordinate systems are defined (Fig. 2). The two systems are defined as the inertial (x_0, y_0, z_0) and body (x_b, y_b, z_b) frame. The centrifugal force vector $\bar{g}_0$ remains fixed relative to the inertial frame. The body frame, with its origin at the center of the tube circles the x_0-axis at a

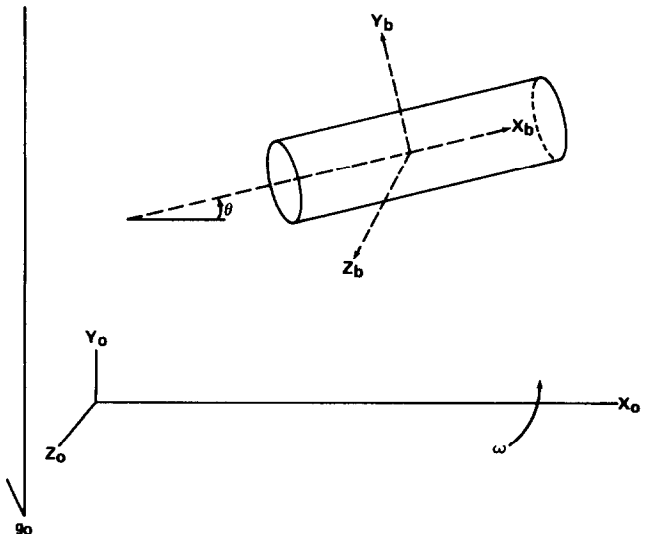

Fig. 2. Rotating coil planet centrifuge (RCPC) cylinder section.

constant angular velocity ω. The x_b-axis of the body frame forms an angle θ with the x_0 inertial frame.

As a first approximation, only two forces are considered to be acting on the spherical particle. These forces are the Stokes drag ($\vec{F}_s$) and centrifugal force ($\vec{F}_{g_0}$). The centrifugal force (g_b) caused by rotation of the body frame about x_0 is much smaller than $\vec{F}_{g_0}$ and is, therefore, neglected. $\vec{F}_s$ and $\vec{F}_{g_0}$ are defined as follows

$$\vec{F}_s = -6\pi r\,\mu\,\vec{V}_p \tag{1}$$

$$\vec{F}_{g_0} = \frac{4}{3}\pi r^3\,(\rho - \rho_0)\,g_0 \tag{2}$$

where, r = particle radius, μ = fluid viscosity, $\vec{V}_p$ = particle velocity relative to fluid, ρ = particle density, ρ_0 = fluid density.

Euler transformations are used to describe g_0 in terms of body coordinates. The body frame is considered to be inertial since g_b is considered negligible. Using this assumption, one can now rotate g_0 about the y_b-axis. In terms of Euler transformations this yields the following expression:

$$\begin{bmatrix} g_{0x} \\ g_{0y} \\ g_{0z} \end{bmatrix}_b = \begin{pmatrix} \cos\theta & 0 & -\sin\theta \\ 0 & 1 & 0 \\ \sin\theta & 0 & \cos\theta \end{pmatrix} \begin{pmatrix} 1 & 0 & 0 \\ 0 & \cos\omega t & \sin\omega t \\ 0 & -\sin\omega t & \cos\omega t \end{pmatrix} \begin{pmatrix} g_{0x} \\ g_{0y} \\ g_{0z} \end{pmatrix}_0 \tag{3}$$

Since rotation is only about the y_b-axis, the x_0 and z_0 components are set to zero.

$$\begin{bmatrix} g_{0x} \\ g_{0y} \\ g_{0z} \end{bmatrix}_b = \begin{pmatrix} \cos\theta & 0 & -\sin\theta \\ 0 & 1 & 0 \\ \sin\theta & 0 & \cos\theta \end{pmatrix} \begin{pmatrix} 1 & 0 & 0 \\ 0 & \cos\omega t & \sin\omega t \\ 0 & -\sin\omega t & \cos\omega t \end{pmatrix} \begin{pmatrix} 0 \\ g_{0y} \\ 0 \end{pmatrix}_0 \tag{4}$$

This reduces to:

$$\begin{bmatrix} g_{0x} \\ g_{0y} \\ g_{0z} \end{bmatrix}_b = g_0 \begin{pmatrix} \sin\theta\,\sin\omega t \\ \cos\omega t \\ -\cos\theta\,\sin\omega t \end{pmatrix} \tag{5}$$

From Newton's second law of motion:

$$\vec{a}_p = \frac{\vec{F}_p}{m_p} \tag{6}$$

where m_p = particle mass, and $\vec{F}_p$ = total particle force, when changing to matrix notation from eqn. 5 one derives at

$$\vec{F}_{g_0} = \begin{bmatrix} F_{g_{0x}} \\ F_{g_{0y}} \\ F_{g_{0z}} \end{bmatrix}_b = m_p g_0 \begin{pmatrix} \sin\theta \sin\omega t \\ \cos\omega t \\ -\cos\theta \sin\omega t \end{pmatrix} \tag{7}$$

Letting $K = 6\pi r\mu$ one sees that,

$$\vec{F}_s = -K\vec{V}_p \tag{8}$$

Now,

$$\vec{F}_p = \vec{F}_{g_0} + \vec{F}_s \tag{9}$$

Describing the lateral particle velocity ($\vec{V}_p$) in matrix notation,

$$\vec{V}_p = \begin{bmatrix} \dot{x} \\ \dot{y} \\ \dot{z} \end{bmatrix}_b \tag{10}$$

and

$$\vec{a}_p = \begin{bmatrix} \ddot{x} \\ \ddot{y} \\ \ddot{z} \end{bmatrix}_b \tag{11}$$

and substituting eqns. 7–11 into eqn. 6 yields

$$\begin{bmatrix} \ddot{x} \\ \ddot{y} \\ \dot{z} \end{bmatrix}_b = \frac{1}{m_p} \left\{ m_p g_0 \begin{pmatrix} \sin\theta \sin\omega t \\ \cos\omega t \\ -\cos\theta \sin\omega t \end{pmatrix} - K \begin{bmatrix} \dot{x} \\ \dot{y} \\ \dot{z} \end{bmatrix}_b \right\} \tag{12}$$

Rearranging terms,

$$\begin{bmatrix} \ddot{x} \\ \ddot{y} \\ \ddot{z} \end{bmatrix}_b + \frac{K}{m_p} \begin{bmatrix} \dot{x} \\ \dot{y} \\ \dot{z} \end{bmatrix}_b = g_0 \begin{pmatrix} \sin\theta \sin\omega t \\ \cos\omega t \\ -\cos\theta \sin\omega t \end{pmatrix} \tag{13}$$

which yields the following differential equations in terms of x_b, y_b, and z_b body coordinates.

$$\dot{V}_{x_b} + \frac{K}{m_p} V_{x_b} = g_0 \sin\theta \sin\omega t \tag{14}$$

$$\dot{V}_{y_b} + \frac{K}{m_p} V_{y_b} = g_0 \cos\omega t \tag{15}$$

$$\dot{V}_{z_b} + \frac{K}{m_p} V_{z_b} = -g_0 \cos\theta \sin\omega t \tag{16}$$

Use of Laplace transforms results in the following solutions for V_x, V_y, and V_z:

$$V_{x_b} = \left(\frac{g_0 \sin\theta}{K}\right)\left[\frac{\left(\frac{\omega}{K}\right)}{1+\left(\frac{\omega}{K}\right)^2} e^{-kt} + \frac{1}{\sqrt{1+\left(\frac{\omega}{K}\right)^2}} \sin(\omega t - \varphi)\right] \tag{17}$$

$$V_{y_b} = \left(\frac{g_0}{K}\right)\left[\frac{-1}{1+\left(\frac{\omega}{K}\right)^2} e^{-kt} + \frac{1}{\sqrt{1+\left(\frac{\omega}{K}\right)^2}} \cos(\omega t - \varphi)\right] \tag{18}$$

$$V_{z_b} = \left(\frac{-g_0 \cos\theta}{K}\right)\left[\frac{\left(\frac{\omega}{K}\right)}{1+\left(\frac{\omega}{K}\right)^2} e^{kt} + \frac{1}{\sqrt{1+\left(\frac{\omega}{K}\right)^2}} \sin(\omega t - \varphi)\right] \tag{19}$$

Integrating the lateral velocities V_{x_b}, V_{y_b}, *and* V_{z_b} with respect to t yields:

$$\int V_{x_b}\,dt = x_b = \left(\frac{g_0 \sin\theta}{K}\right)\left\{\left[\frac{\left(\frac{\omega}{K}\right)}{1+\left(\frac{\omega}{K}\right)^2}\right]\left(\frac{-e^{-kt}}{K}\right) + \left[\frac{1}{\sqrt{1+\left(\frac{\omega}{K}\right)^2}}\right]\left[\frac{\cos(\omega t - \varphi)}{\omega}\right]\right\} + C_x \tag{20}$$

$$\int V_{y_b}\,dt = y_b = \left(\frac{g_0}{K}\right)\left\{\left[\frac{-1}{1+\left(\frac{\omega}{K}\right)^2}\right]\left(\frac{-e^{-kt}}{K}\right) - \left[\frac{1}{\sqrt{1+\left(\frac{\omega}{K}\right)^2}}\right]\left[\frac{\sin(\omega t-\varphi)}{\omega}\right]\right\} + C_y \tag{21}$$

$$\int V_{z_b}\,dt = z_b = \left(\frac{-g_0\cos\theta}{K}\right)\left\{\left[\frac{\frac{\omega}{K}}{1+\left(\frac{\omega}{K}\right)^2}\right]\left(\frac{-e^{kt}}{K}\right) + \left[\frac{1}{\sqrt{1+\left(\frac{\omega}{K}\right)^2}}\right]\left[\frac{\cos(\omega t-\varphi)}{\omega}\right]\right\} + C_z \tag{22}$$

After determining a particle's position within the cylinder, one can assign an axial velocity given the following flow velocity relation,

$$V(y) = 3/2\ V_{av}\left(1-\frac{y^2}{b^2}\right) \tag{23}$$

where b = cylinder radius, y = particle distance from center, V_{av} = average fluid velocity. Fig. 3 shows the parabolic flow velocity profile generated by eqn. 23 in a 1-mm I.D. tube at a fluid flow-rate of 15 ml/h. Velocities are now averaged over a 2π radian period resulting in the particles average fluid attributed velocity V_f. Total particle velocity V_T is obtained by summing V_f and V_{x_b}.

RESULTS AND DISCUSSION

Fig. 4 shows the cross-sectional displacements for sheep and human erythrocytes at a fixed helical rotation rate of 4 rpm in a centrifugal force of 142 g. The particle path in the x_b–y_b plane is elliptical. Because of the overlapping elliptical path, there is a resulting net zero particle velocity along the x_b axis ($2V_{x_b} = 0$) attributable to the centrifugal force F_{g_0}. The integration constants C_x, C_y and C_z in eqns. 20–22 represent offsets from the tube centerline. The model is based on the trajectories of single particles, hence no compensation is made for interactions among separate particles. A statistical analysis of a fixed population of ideal particles involving a more rigorous treatment of particle interactions is to be the subject of a future paper. Also involved in this statistical model will be the initial random distribution of par-

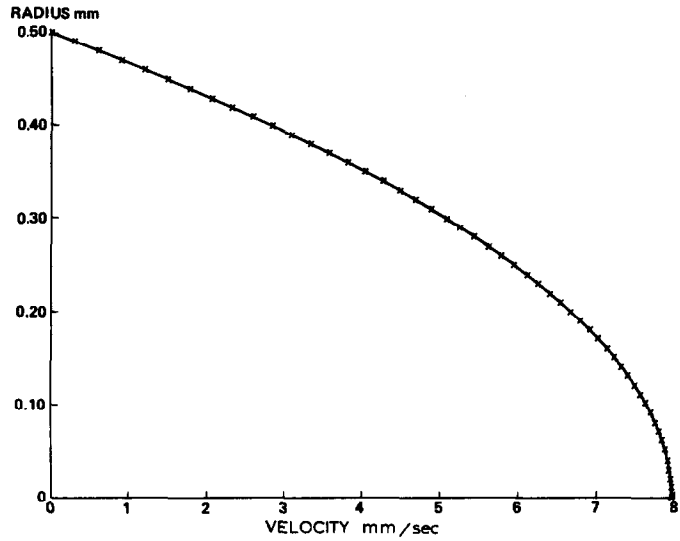

Fig. 3. Laminar velocity profile (15 ml/h).

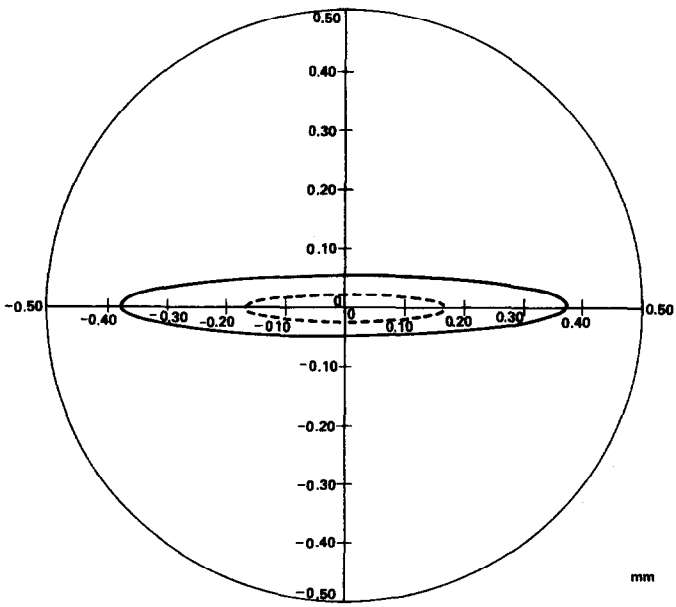

Fig. 4. Cell dynamics in RCPC separation. (———), Human erythrocytes (retention time = 141 min); (---------), sheep erythrocytes (retention time = 107 min). Rotation = 4 rpm; flow-rate = 11.1 ml/h; centrifugal force = 142 *g*; isotonic phosphate buffer.

ticles within the tube and any subsequent ordering of particles which might be the result of the rotating coil planet centrifuge process.

The present model assumes a net zero particle axial velocity during the time that the particle remains in contact with the column wall. By making this assumption, one neglects axial particle velocities which are the result of Archimedean screw forces (*i.e.* particle roll along the helical column wall).

Fig. 5 shows the predicted relationship between the centrifugal force field and particle retention times at a fixed helical coil rotation rate of 4 rpm. Fig. 6 illustrates the relationship between the retention time and helical coil rotation rate.

Fig. 7 shows experimental fraction retention times for a mixture of fresh sheep and human erythrocytes. The corresponding adsorbption data (recorded at 280 nm) are shown in Fig. 8.

Within the limits of the nonstatistical solution presented here, the results predicted agreed well with the experimental data obtained. In light of the liberal assumptions made, which disregard actual particle shapes and concentration effects of particles, one sees that the solutions adequately describe the synergetic efects of sedimentation rates and flow gradients of particle separations in the coil planet centrifuge at low helical coil rotation rates.

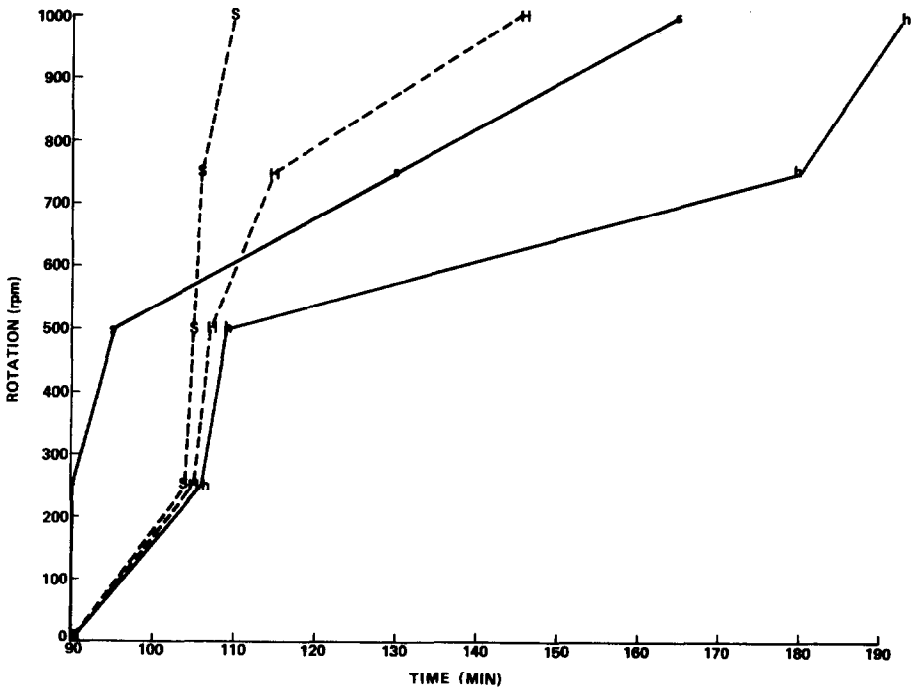

Fig. 5. Actual and predicted RCPC retention times of sheep and human erythrocytes, plotted as a function of centrifugal field. Rotation corresponds to operational centrifugal force. (——— h), Human erythrocytes actual; (———s), sheep erythrocytes actual; (--------- H), human erythrocytes predicted; (--------- S), sheep erythrocytes predicted. Flow-rate = 8.7 ml/h; rotation = 4 rpm.

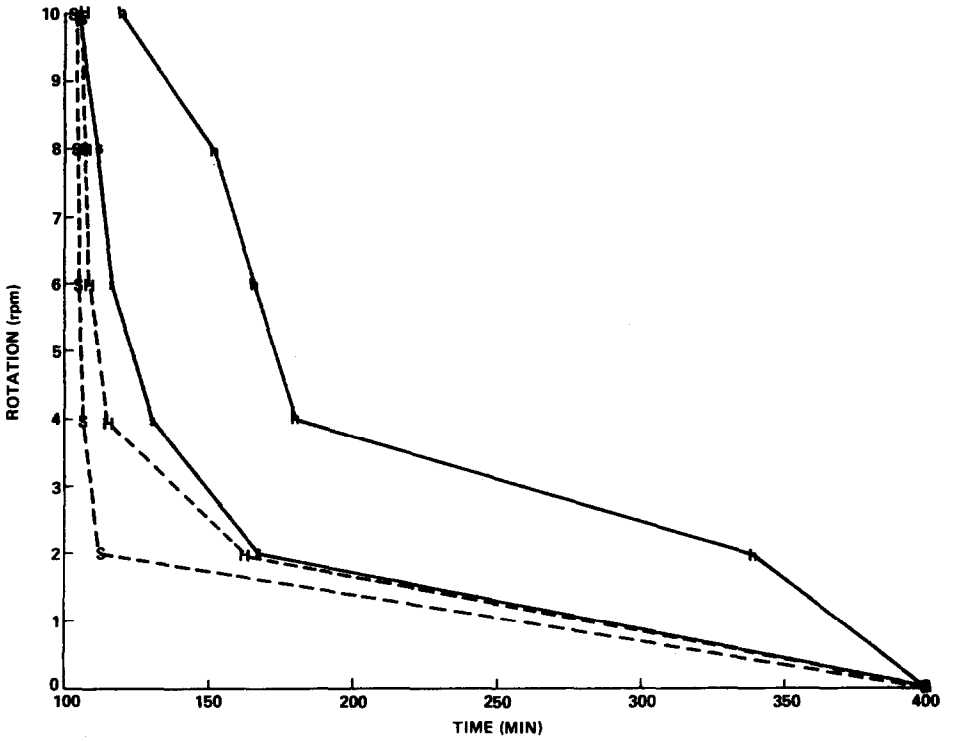

Fig. 6. Actual and predicted RCPC retention times of sheep and human erythrocytes, plotted as a function of rotational rate. (——— h), human erythrocytes actual; (——— s), sheep erythrocytes actual; (--------- H), human erythrocytes predicted; (--------- S), sheep erythrocytes predicted. Flow-rate = 8.7 ml/h; centrifugal force = 75 *g*.

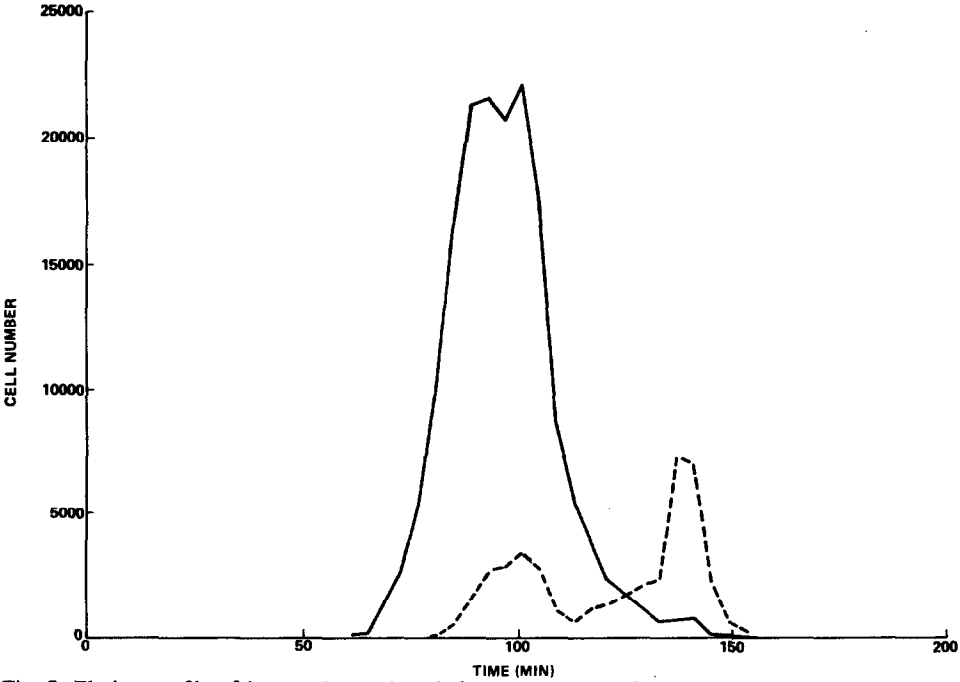

Fig. 7. Elution profile of human (---------) and sheep (———) erythrocytes with the nonsynchronous flow-through coil planet centrifuge. Flow-rate = 15 ml/h; rotation = 4 rpm; centrifugal force = 142 *g*.

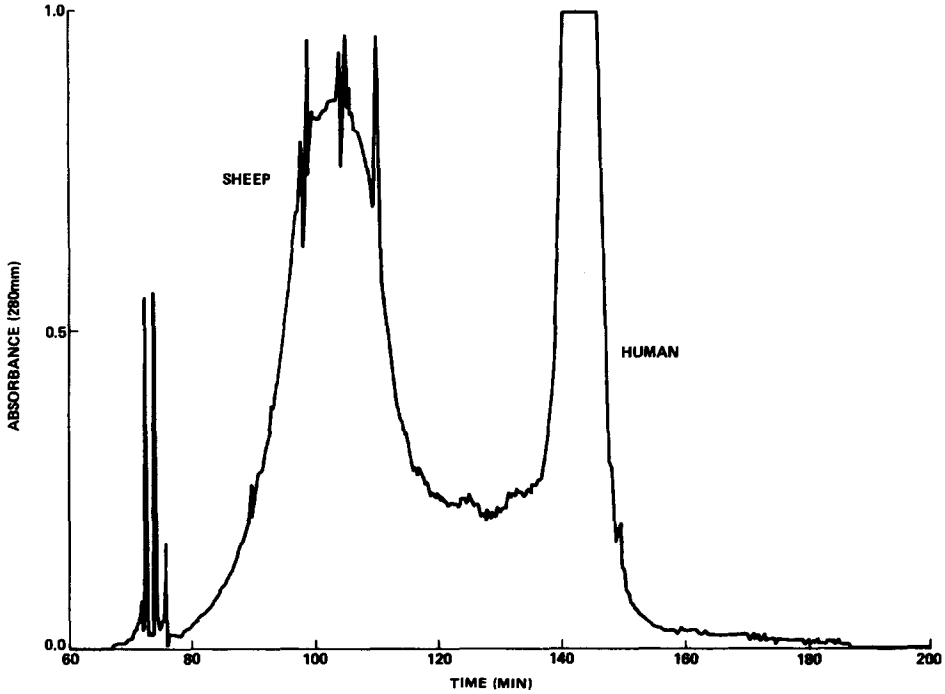

Fig. 8. Typical UV absorption curve of human and sheep erythrocytes separated on the rotating coil planet centrifuge. Conditions as in Fig. 7.

ACKNOWLEDGEMENTS

I wish to acknowledge the aid given by Dr. Yoichiro Ito of the National Institutes of Health at Bethesda (MD, U.S.A.) in the loan of his coil planet centrifuge. I would also like to express my appreciation to Dr. Robert Snyder and Mr. Douglas Nixon of NASA at the Marshall Space Flight Center for their direction of this work and to Ms Helen Matsos for her assistance in the operation of the rotating coil planet centrifuge.

REFERENCES

1 Y. Ito, P. Carmeci, R. Bhatnagar, S. Leighton and R. Seldon, *Sep. Sci. Technol.*, 15 (1980) 1589–1598.
2 Y. Ito, G. T. Bramlett, R. Bhatnagar, M. Huberman, L. L. Leive, L. M. Cullinane and W. Groves, *Sep. Sci. Technol.*, 18 (1983) 33–48.
3 Y. Ito, P. Carmeci and I. A. Sutherland, *Anal. Biochem.*, 94 (1979) 249–252.
4 Y. Ito, M. Weinstein, I. Aoki, R. Harada and E. Kimura, *NASA*, 212 (1966) 985–987.